J Mater Sci: Mater Med (2011) 22:1511–1519
DOI 10.1007/s10856-011-4332-5

In vitro biological and tribological properties of transparent magnesium aluminate (Spinel) and aluminum oxynitride (ALON®)

Subhadip Bodhak · Vamsi Krishna Balla · Susmita Bose · Amit Bandyopadhyay · Uday Kashalikar · Santosh K. Jha · Suri Sastri

Received: 20 December 2010 / Accepted: 27 April 2011 / Published online: 12 May 2011

Abstract The purpose of this first generation investigation is to evaluate the in vitro cytotoxicity, cell-materials interactions and tribological performance of Spinel and ALON® transparent ceramics for potential wear resistant load bearing implant applications. Besides their non-toxicity, the high surface energy of these ceramics significantly enhanced in vitro cell-materials interactions compared to bioinert commercially pure Ti as control. These transparent ceramics with high hardness in the range of 1334 and 1543 HV showed in vitro wear rate of the order of 10^{-6} mm^3 Nm^{-1} against Al_2O_3 ball at a normal load of 20 N.

1 Introduction

Total hip arthroplasty (THA) and total knee arthroplasty (TKA) are the most clinically successful interventions in health care, with numerous investigations reporting excellent long-term results in terms of reducing pain, improving functionality and quality of life in patients with debilitating hip/knee diseases [1–3]. However, despite continuous improvement in implant materials, designs and surgical techniques, the number of revision arthroplasty cases in the United States is still very high [4]. Recent statistics of THA/TKA [5, 6] further suggests that significant research efforts are needed to improve materials, surfaces and designs for load bearing implants. The most common reason for bone loss and therefore aseptic loosening is implant-derived wear particles, and other wear products, which induce a foreign body inflammatory response in the joint capsule and along implant–bone interfaces.

For THA/TKA implants, Co-based alloys are common because of their excellent mechanical and wear properties [7]. However, the release of metal ions in vivo is still a serious concern for these Co-based alloys in load bearing implants. Klapperich and co-workers [8] reported incidents of metal-on-metal total hip arthroplasty failures as a result of progressive osteolysis. Although the ultra high molecular weight polyethylene (UHMWPE)-on-metal bearings are extremely durable and have performed well in the vast majority of patients, surgeons are more conservative about performing these procedures in younger patients, as patient weights and expectations concerning any activity limitations are different from those today. As patient demand for the procedure increases, and the average age at which a THA is decreasing, the problems with implant failure can further be magnified in the future. It has been shown that ceramic-on-ceramic types of devices exhibit significantly lower wear rates than other material combinations such as metal-on-metal and metal-on-polyethylene [9–11].

Use of ceramic-on-ceramic articulations can further eliminate the UHMWPE liner and allow a larger diameter femoral heads for a given acetabular diameter, which can increase the range of motion and also reduce the risk of instability/dislocation—a major cause for revision surgery [9]. The ceramic-on-ceramic configurations showed extremely low wear rates [10] and good survival rates [11]. In addition, the ceramics can readily chemisorbs lubricating

S. Bodhak · V. K. Balla · S. Bose · A. Bandyopadhyay (✉)
W. M. Keck Biomedical Materials Research Laboratory, School of Mechanical and Materials Engineering, Washington State University, Pullman, WA 99164-2920, USA
e-mail: amitband@wsu.edu

S. Bodhak
JSPS Postdoctoral Researcher, Biomaterials Center, National Institute for Materials Science (NIMS), Tsukuba, Japan

U. Kashalikar · S. K. Jha · S. Sastri
Surmet Corporation, Burlington, MA, USA

compounds due to their higher surface energy and wettability providing low friction surface compared to metals [12, 13]. Compared to other ceramics such as Al_2O_3 and ZrO_2 used for load bearing orthopedic applications, aluminum oxynitride ($Al_{23}O_{27}N_5$, AlON), and magnesium aluminate ($MgAl_2O_4$, Spinel) ceramics offer high processing flexibility in terms of achieving full density and complex shaped implant components, with comparable hardness and fracture toughness. Spinel found to exhibit R-curve behavior [14, 15] and does not show substantial subcritical crack growth behavior [16], which suggests its superior resistance to service or processed induced flaws. Superior wear resistance has also been reported for Al_2O_3 when reinforced with AlON [17]. Whereas, Al_2O_3 usually suffer from subcritical crack growth behavior and in vivo metastability/polymorphic transformation of ZrO_2 and stresses arising from that strongly affect ZrO_2's structural performance [18–20]. Finally, the transparent nature of ALON® and Spinel ceramics enable possible optical monitoring of micro/macro defects and implant fixation/cellular activity. Therefore, in this work we have explored the potential for commercially available transparent Spinel and ALON® ceramics towards load bearing implant applications and evaluated their in vitro tribological and biological properties.

2 Materials and methods

Transparent ceramic discs (99.7–99.8% pure) with ϕ 25.2 mm namely, Spinel ($MgAl_2O_4$) and ALON® ($Al_{23}O_{27}N_5$) having 1.2 and 2.1 mm thickness, respectively were processed at Surmet Corporation (Burlington, MA, USA) and used in this study. The samples were made following conventional powder processing route, i.e., dry isostatic pressing followed by sintering and final grinding and polishing to achieve optically smooth surface finish (surface roughness (r.m.s) = ~0.001 μm). The relative density of present samples was between 99.49 and 99.62%. These transparent ceramics were evaluated for their in vitro tribological properties and bone cell-materials interactions.

2.1 Tribological properties

One of the main causes of the aseptic loosening may be attributed to fretting wear in the joint, where the released wear debris stay inside the contact and/or spread around the prosthesis. Recently it has been shown that sliding wear between two articulating surfaces under normal loading condition is one of the major factors causing the loosening of joint prostheses [21]. Therefore, linear reciprocating ball-on-disc wear testing, according to ASTM G133, was performed using a tribometer (NANOVEA, Microphotonics Inc., CA, USA) with ϕ 3 mm Al_2O_3 ball rubbing against Spinel and ALON® test samples. We have chosen Al_2O_3 as counter articulating material due to non-availability of commercial Spinel and ALON® balls. As shown in Fig. 1, the test samples had superfine optically smooth surface finish (surface roughness (r.m.s) = ~0.001 μm) in as-received condition and therefore, no further surface preparation steps were used. However, before starting the wear tests, these samples and counter Al_2O_3 ball were ultrasonically cleaned in acetone. In all wear experiments, a constant linear oscillatory motion of 10 mm in length (the full cycle represents 20 mm of travel) with a constant speed of 5000 mm/min and constant normal load of 20 N were used. The sliding speeds used in the present work are significantly higher than the sliding speeds during a walking cycle in a total hip prosthesis with 28 mm diameter [22] and are so chosen to study the wear rate under extreme conditions. Similarly, under 20 N normal load, the initial maximum Hertzian contact pressure was found to be 3.42 and 3.59 GPa for Spinel and ALON® samples, respectively, and such a contact pressure is a result of a hip joint peak loads up to 5 times the body weight during level walking [23]. The wear rate of each test samples was calculated as $mm^3\ Nm^{-1}$ for 1000 and 3000 m of sliding distance. All tests were carried out in aseptic condition in freshly prepared simulated body fluid (SBF) at 37°C. We have selected SBF as a test medium based on several earlier reports, where SBF has been used as an articulating media to simulate wear on joint replacement devices [24–27]. Although the addition of proteins to SBF can change the wear behavior, present wear tests in SBF can also quantify the response of present articulation surfaces under present experimental loading conditions. The ionic concentrations of the SBF used in present study are as follows: 2.5 mM of Ca^{2+}, 1.5 mM of Mg^{2+}, 142.0 mM of Na^+, 5.0 mM of K^+, 147.8 mM of Cl^-, 4.2 mM of HCO_3^-, 1.0 mM of HPO_4^{2-},

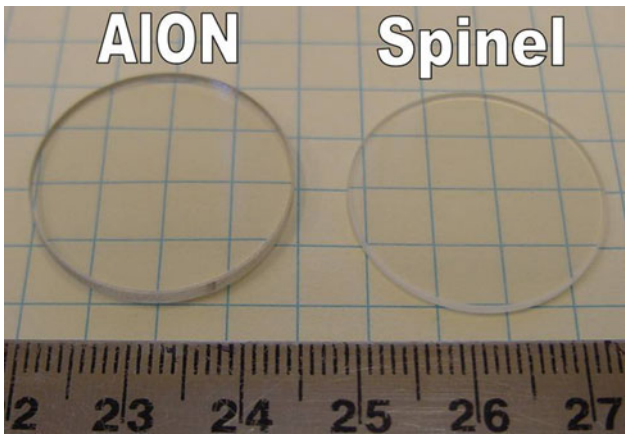

Fig. 1 As-received ALON® and Spinel samples showing transparency and superfine optically smooth surface finish

0.5 mM of SO_4^{2-}. The top surface hardness of the test samples was measured using a Vickers microhardness tester (Shimadzu, HMV-2T) at 300 g load for 15 s and the average value of 7 measurements was reported.

2.2 Contact angles and surface energy

The surface energy of as-received Spinel and ALON® samples was calculated from experimentally determined contact angles. Prior to the test, all the samples were ultrasonically cleaned in an alcohol bath. Contact angles were measured using the sessile drop method with a face contact angle setup equipped with a microscope and a camera. Images were collected with the camera and the contact angle between the drop and the substrate was measured from the magnified image. For each sample and liquid combination, an average of 6 measurements is reported. Surface energy of transparent ceramic samples was calculated based on contact angle measurements, which were conducted with two liquids with polar and non-polar characteristics: distilled water and diiodomethane. In this study, Fowkes' equation was used to calculate the energy [28]:

$$\frac{\gamma_L(1+Cos\theta)}{2} = \sqrt{\gamma_L^d \gamma_S^d} + \sqrt{\gamma_L^p \gamma_S^p} \quad (1)$$

$$\gamma_S = \gamma_S^d + \gamma_S^p \quad (2)$$

where, γ_s is the total surface energy of solid, γ_L is the total surface tension of liquid, γ_s^d and γ_s^p are respectively the dispersive and polar components of the solid surface energy. Equation 1 was used to calculate dispersive (γ_s^d) and polar (γ_s^p) components of solid surface energy from the contact angle measurements with diiodomethane and distilled water, respectively. Equation 2 was used to calculate the total surface energy of the solid ($\gamma_s^d + \gamma_s^p$).

2.3 In vitro bone cell-materials interactions

In vitro cytotoxicity behavior of Spinel and ALON® samples was evaluated for a maximum incubation period of 5 days using human fetal osteoblast cell (hFOB) line (CRL-11372, ATCC, VA, USA). Each sample (3 samples for each composition and culture duration) was sterilized by autoclaving at 121°C for 20 min prior to cell culture experiment. Following this, cells were seeded onto sample surfaces, placed in a 6-well plate. 4 ml of DMEM cell media enriched with 10% fetal bovine serum was added to each well. Cultures were maintained in an incubator at 37°C under an atmosphere of 5% CO_2 and 95% air. The culture media were changed every alternate day.

Cell morphology on test samples was assessed after 3 and 5 days of incubation period using SEM. Cultured samples for SEM observation were rinsed with 0.1 M phosphate-buffered saline (PBS) and fixed with 2% paraformaldehyde/2% glutaraldehyde in 0.1 M cacodylate buffer overnight at 4°C. Following this, post fixation for each sample was made with 2% Osmium tetroxide (OsO_4) for 2 h at room temperature. Fixed samples were then dehydrated in an ethanol series 30, 50, 70, 95 and 100% three times, each followed by a hexamethyldisilane (HMDS) drying procedure. Dried samples were then mounted on aluminum stubs, gold coated and observed under an FESEM.

The proliferation of viable hFOB cells attached on the sample surfaces after 3 and 5 days of incubation period was assessed by the MTT assay (Sigma, MO, USA). For comparison, polished commercially pure Ti (CP-Ti, 99.9% purity, (surface roughness (r.m.s) = 0.0074 ± 0.0001 μm) was used as a control. Five samples for each composition and culture duration were used to evaluate cell proliferation using MTT assay. MTT solution [3-(4,5-Dimethylthiazol-2-yl)-2,5-diphenyl tetrazolium] of 5 mg/ml was prepared by dissolving MTT in PBS, and filter sterilized. MTT solution was diluted (i.e. 400 μl MTT solution into 3.6 ml DMEM culture media enriched with 10% fetal bovine) and added to each sample to form formazan by mitochondrial dehydrogenases. After 2 h incubation at 37°C, samples were transferred to a new 6-well plate and 4 ml of solubilization solution made up of 10% Triton X-100, 0.1 N HCl and isopropanol were added to dissolve the formazan crystals. Then 100 μl of the resulting supernatant was transferred into a 96-well plate and three data points were obtained from each sample. The optical density of the solution in each well was measured at a wavelength of 570 nm using a microplate reader (Cambridge Tech., MA, USA). In the MTT assay study, polished CP-Ti (surface roughness (r.m.s) = 0.0074 ± 0.0001 μm) was used as a control sample.

2.4 Statistical analysis

Data for wear rate, Vickers microhardness, contact angle, surface energy and MTT assay are presented as mean ± standard deviation. Statistical analysis was performed on MTT assay results using Student's t test and P value <0.05 was considered significant.

3 Results and discussion

3.1 Wear rate and hardness

In vitro wear rate, in $mm^3\ Nm^{-1}$, of ceramic discs was calculated from the wear track dimensions measured using SEM images of the worn discs. Table 1 shows the influence of sliding distance on the wear volume of Spinel and ALON®

Table 1 Wear rate ($\times 10^{-6}$ mm^3 Nm^{-1}), volume loss (mm^3) and surface hardness (HV) of transparent Spinel and ALON® samples

Sample	Wear rate		Volume loss		Hardness
	1000 m	3000 m	1000 m	3000 m	
Spinel	4.72 ± 1.22	5.27 ± 0.85	0.094 ± 0.02	0.316 ± 0.05	1334.57 ± 73.03
ALON®	12.5 ± 2.16	10.1 ± 0.27	0.250 ± 0.01	0.606 ± 0.03	1543.85 ± 47.30

samples. The wear volume of Spinel and ALON® samples was found to be in the range of 0.094–0.316 and 0.250–0.606 mm^3, respectively. The wear volume increased with increasing sliding distance for both the samples. At both sliding distances of 1000 and 3000 m the ALON® samples showed higher volume loss than Spinel samples. Figure 2 shows experimentally determined wear rate of transparent Spinel and ALON® samples for sliding distances up to 3000 m. Experimental data clearly indicate that Spinel has superior wear resistance compared to ALON®. From Fig. 2, it can be seen that after 1000 m sliding, ALON® sample exhibited roughly three times higher wear rate ($\sim 12.5 \times 10^{-6}$ mm^3 Nm^{-1}) than Spinel, which showed a lower wear rate of 4.7×10^{-6} mm^3 Nm^{-1}. A small increase in the wear rate to $\sim 5.3 \times 10^{-6}$ mm^3 Nm^{-1} was observed for Spinel with an increase in sliding distance from 1000 to 3000 m although the statistical analysis revealed that this difference is not significant. Interestingly, after 3000 m sliding distance, ALON® exhibited a reduction in wear rate ($\sim 10 \times 10^{-6}$ mm^3 Nm^{-1}), which is two times higher than what observed for Spinel under identical wear test conditions. In general, materials exhibit high initial running-in wear rate. It was observed that with an increase in the sliding distance, the wear rate gradually decreases and reaches at a constant value (steady-state wear regime) [29]. Fig. 3 shows the variation of friction coefficient of Spinel ALON® surfaces against Al_2O_3. For 1000 m sliding distance tests the coefficient of friction for Spinel was found to increase from 0.31 to 0.44 (average: 0.42 ± 0.02) and for ALON® it increased from 0.37 to 0.48 (average: 0.45 ± 0.02). The results of 3000 m sliding distance (Fig. 3) show that the friction coefficient of ALON® gradually increased and appears to reach steady state at ~1700 m sliding distance. The Spinel samples showed a small decrease in the coefficient of friction from ~0.45 to 0.42 around 500 m sliding distance, which remained more or less constant up to 3000 m sliding distance. From these results it appears that ALON® and Spinel samples reached steady-state wear regime after approximately 1700 m and 500 m sliding distance, respectively. The lower wear rate of Spinel than ALON® correlates with their respective friction coefficients, i.e., 0.43 ± 0.009 for Spinel and 0.46 ± 0.02 for ALON®.

The wear rate of the order of 10^{-6} mm^3 Nm^{-1} observed on present materials is significantly lower than ZrO_2 sliding against ZrO_2, which showed a wear rate of 10^{-4} to 10^{-3} mm^3 Nm^{-1} under test conditions close to present experimental conditions [30]. Another study on sliding wear of plasma sprayed Al_2O_3 coatings on mild steel showed a wear rate between 3.5 and 9.5×10^{-3} mm^3 Nm^{-1} when tested against Al_2O_3 balls [31]. Recent study on wear simulation of Al_2O_3-on-Al_2O_3 prosthetic hip joints using a multidirectional motion pin-on-disk device showed that the wear rate of Al_2O_3 is of the order of 10^{-8} mm^3 Nm^{-1} [32], which is significantly lower than the wear rates of Spinel and ALON® used in the present work. However, it is

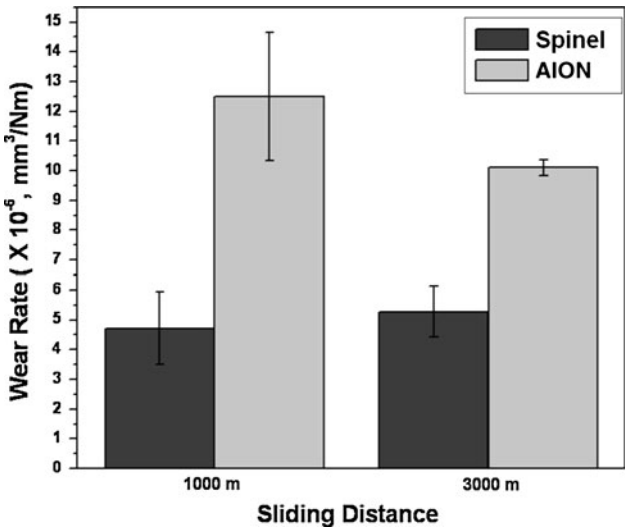

Fig. 2 Wear rate of Spinel and ALON® samples after 1000 and 3000 m sliding distance

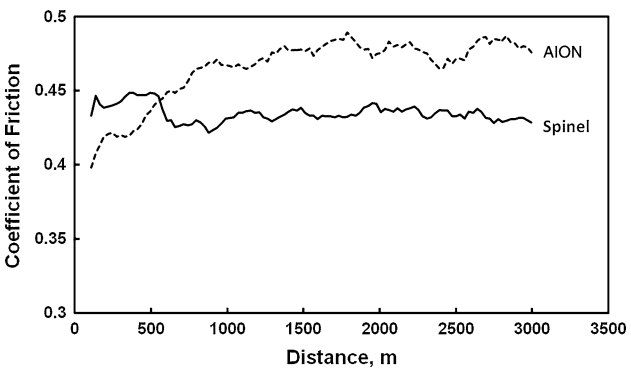

Fig. 3 Variation of coefficient of friction as a function of sliding distance

important to note that the present experimental conditions, with initial maximum Hertzian contact pressure of 3.42 and 3.59 GPa for Spinel and ALON® samples, respectively, are close to severe wear region of Al_2O_3 wear, where the wear rate of Al_2O_3 has been shown to be of the order of 10^{-5} to 10^{-4} mm^3 Nm^{-1} [33]. In the earlier work [32] on wear simulation of Al_2O_3-on-Al_2O_3 pins with 26.83 mm radius were used against Al_2O_3 disks with a normal load of 1 N corresponding to a initial maximum Hertzian contact pressure of only 220 MPa. Therefore, the present Spinel transparent ceramics with a wear rate of $\sim 5.3 \times 10^{-6}$ mm^3 Nm^{-1} show significantly higher wear resistance and have potential to be use wear resistant load bearing implant applications.

Table 1 show that the average hardness of Spinel was 1334 HV, while ALON® has relatively high hardness of 1543 HV. Generally the wear resistance of a material has been directly related to its hardness, i.e., higher the hardness higher the wear resistance. However, there are specific situations and materials where hardness has been shown not to correlate with wear [34–37]. Although the observed difference in wear behavior between the two ceramics is not fully understood yet, but high magnification SEM images of the worn tracks clearly indicates more wear on ALON® surface. Fig. 4 illustrates the worn surfaces of both Spinel and ALON® samples after 3000 m sliding. Evidently, an evenly worn deep track with distinct boundaries is clearly visible on ALON® surface (Fig. 4b, d) compared to a relatively shallow and smoother worn track observed on Spinel surface (Fig. 4a, c). From the high magnification SEM images of the worn tracks, parallel arrays of fatigue cracks, oriented perpendicular to sliding direction, were observed on both samples' surface indicating fatigue type wear. Often such tiny microcracks coalesce to form a longer crack, one of such evidences can be found in Fig. 4d. However the degree of flaking and formation of wear debris are appeared to increase and become more visible on ALON® surface (Fig. 4d). Earlier investigations indicate that the dominant wear mechanism of ZrO_2 sliding against ZrO_2 [30] and Al_2O_3 sliding against plasma sprayed Al_2O_3 coatings was abrasion and brittle fracture. The high wear resistance of present transparent ceramics compared to ZrO_2 [30] and plasma sprayed Al_2O_3 [31] is believed to be due to formation of lubricating films on the articulating surfaces during the wear tests performed in SBF, while in the earlier investigations the tests were performed in air (dry wear). Another study on wear simulation of Al_2O_3-on-Al_2O_3 prosthetic hip joints using a

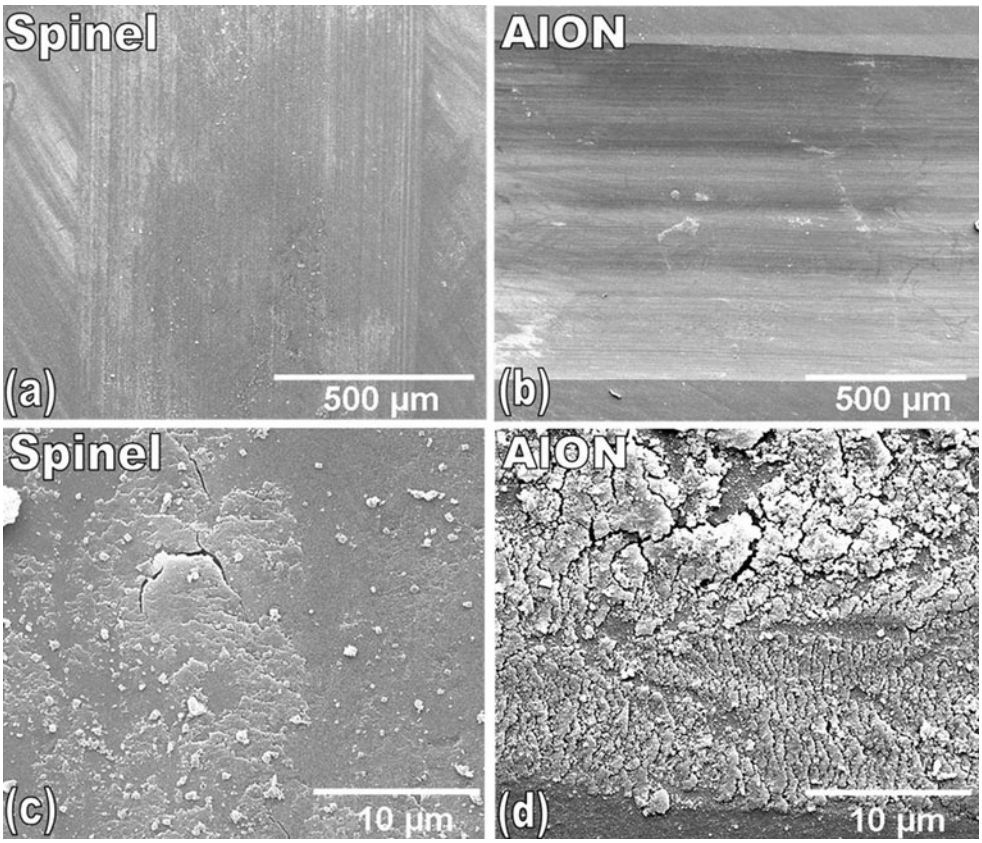

Fig. 4 Wear track morphology after 3000 m of sliding distance (**a**) Spinel and (**b**) ALON® samples. High magnification SEM images of worn areas for (**c**) Spinel and (**d**) ALON® samples

multidirectional motion pin-on-disk device in distilled water and calf serum [32] also showed mild abrasion as dominating wear mechanism. Finally, the differences in surface roughness/preparation of present materials and that of materials used in the earlier investigations [30–32] could have also contributed to the observed differences in the wear mechanisms and wear rates.

3.2 In vitro bone cell-materials interactions

In Fig. 5, sample surfaces imaged after 3 days of culture to investigate bone cell attachment, and spreading on different surfaces are shown. On both Spinel (Fig. 5a, b) and ALON® sample (Fig. 5c, d) surfaces, hFOB cells were found to assume a flat spread shape morphology and well attached to the samples. Here, it can be recalled that osteoblasts are attachment-dependent cells, i.e., they must attach first on the surface then spread and mineralize their extracellular matrix. Dense growth of cells on both the surfaces with numerous cell–cell contacts clearly suggests that Spinel and ALON® surfaces are biocompatible and cause no inhibition to bone cells (hFOB) adhesion and growth. Interestingly, the formation of small white granular apatite nodules on cell surface as observed from the high magnification SEM image (Fig. 5b) indicates that cells are becoming matured on Spinel surface. FESEM images of samples cultured for 5 days are presented in Fig. 6 to show the cell proliferation and early-stage cell differentiation. On Spinel surfaces, cells formed a confluent layer covering the entire surface as shown in Fig. 6a, b. Cells are seen to adhere to each other with cellular micro extensions and connected to substrate in addition to the neighboring cells (Fig. 6b). On ALON® surfaces, cell growth was observed to be less pronounced in comparison to Spinel surface. From a low magnification image (Fig. 6c), it can be clearly seen that cells are still in the process of confluent layer formation on ALON® unlike Spinel surface (Fig. 6b), where cells have already started to mineralize their extracellular matrix with the abundance deposition of apatite minerals [38, 39].

hFOB cell proliferation on both Spinel and ALON® samples has been studied using MTT assay. Commercially pure Ti (CP-Ti), which is one of the most widely used metallic biomaterial, was used as a control sample in an attempt to compare in vitro biocompatibility with that of proposed transparent Spinel and ALON® ceramic samples. MTT assay is a measure of mitochondrial activity that reduces MTT to formazan dye giving purple color. The optical density of the solution is a measure to quantify the cell

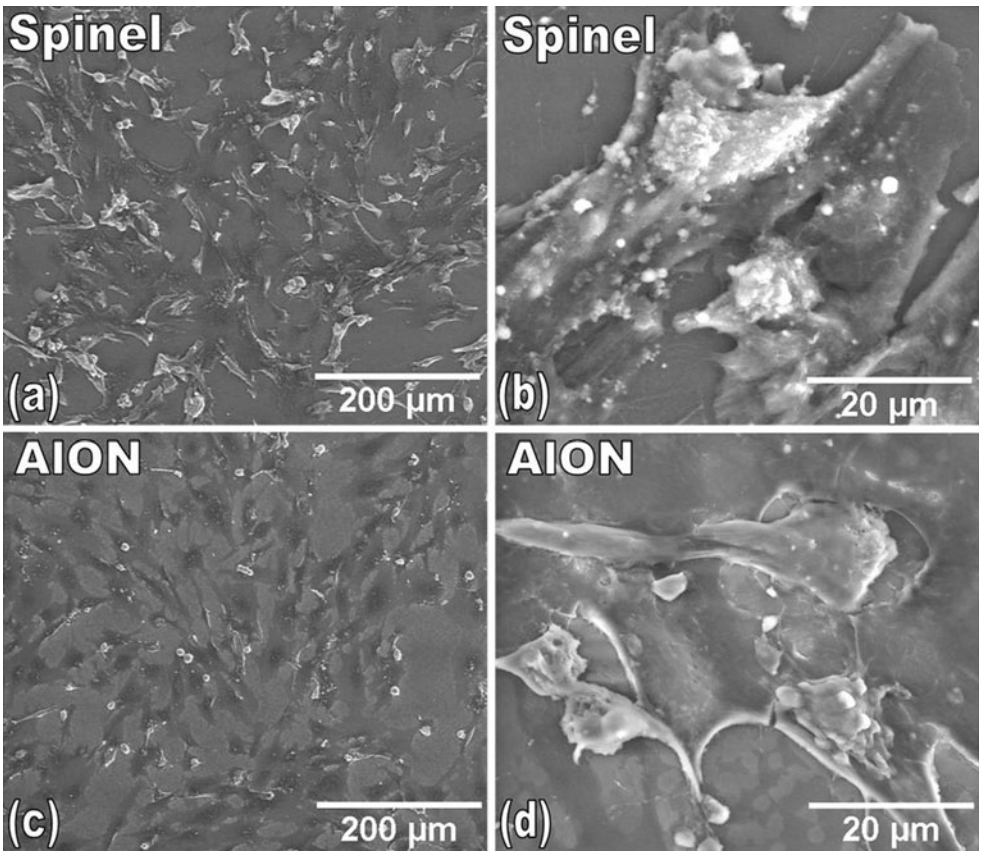

Fig. 5 SEM micrographs showing the cell adhesion after 3 days of culture on Spinel (**a**, **b**) and ALON® (**c**, **d**) sample surfaces

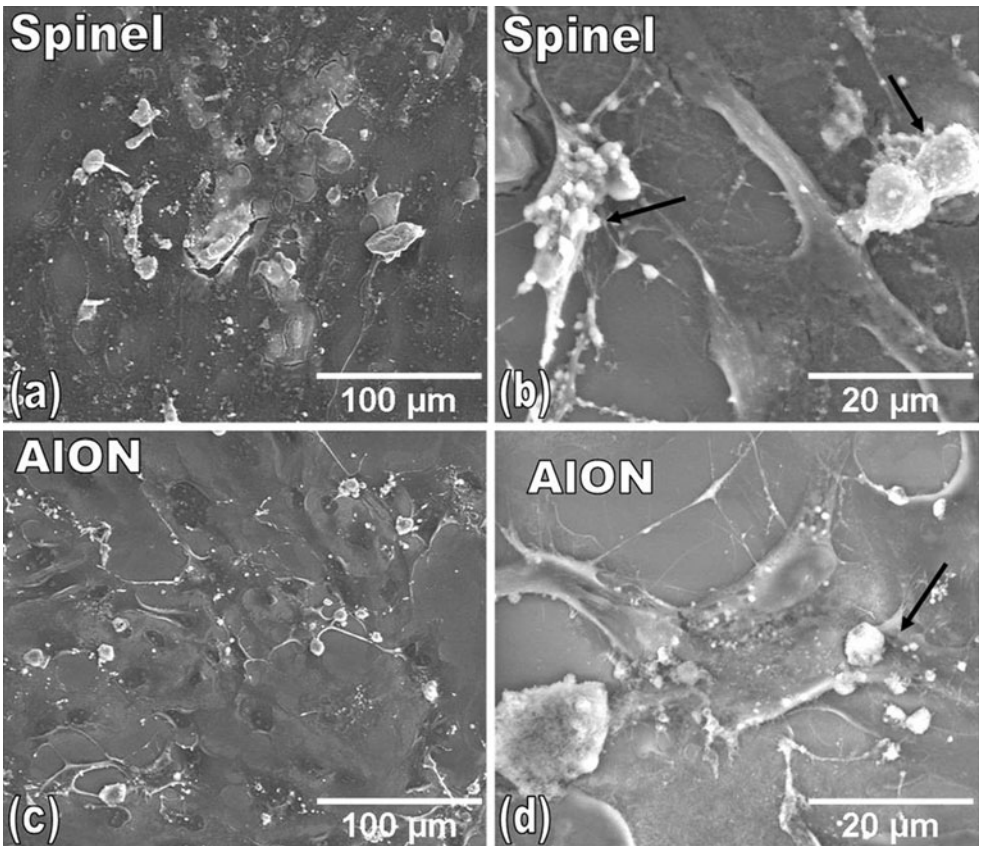

Fig. 6 SEM micrographs illustrating the cell adhesion and proliferation after 5 days of culture on Spinel (**a**, **b**) and ALON® (**c**, **d**) sample surfaces. *Arrows* in high magnification SEM images indicate apatite mineral formation

viability/living cell count on the surface using MTT assay. A higher optical density represents a higher concentration of living cells. In case of human osteoblast cells, a higher number of living cells relates to better biocompatibility of a material. Fig. 7 compares the cell density observed on different samples after 3 and 5 days of culture. Both the Spinel and ALON® samples exhibited excellent biocompatibility and superior growth kinetics of osteoblast cells in comparison to CP-Ti sample for both 3 and 5 day data points. Among the two ceramics, it can be seen that cell proliferation is always higher on Spinel surfaces than on ALON®, and significant difference in mean optical density is always present as confirmed by Student *t* test.

The cell attachment and growth are primarily associated with material's chemistry and surface characteristics such as roughness, wettability and surface energy. Since both the samples used in the present work had superfine optically smooth surface finish (Fig. 1, 0.001 μm) comparable to polished CP-Ti sample (0.007 μm), we hypothesize that the cellular activities on these samples are more of materialistic phenomenon rather than due to surface roughness. Recently, it has also been reported that the surface energy

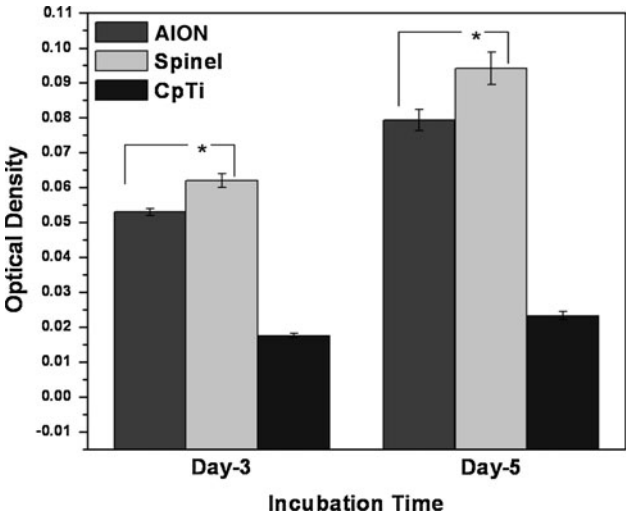

Fig. 7 Optical density measurement illustrating hFOB cell proliferation on Spinel, ALON®, and control Cp-Ti samples. A higher optical density represents a higher concentration of living cells and better biocompatibility. Statistical analysis indicates that the differences in cell densities among Spinel and ALON® samples are significant ($*P < 0.05$, $n = 5$) for both day-3 and day-5 incubation periods

Table 2 Contact angles (°), polar and dispersive components of total surface energy (mN m^{-1}) of transparent Spinel and ALON® sample surfaces

Surface	Distilled water	Diiodomethane	Polar component (γ^p)	Dispersive component (γ^d)	Total surface energy
Spinel	55.3 ± 2.31	48.8 ± 1.16	18.68 ± 4.81	34.96 ± 0.64	53.64 ± 1.15
ALON®	49.3 ± 1.29	48.5 ± 1.12	20.70 ± 1.02	35.11 ± 0.62	55.81 ± 0.65
CP-Ti	69 ± 1.5	55.0 ± 3.0	10.91 ± 1.90	31.38 ± 0.59	42.29 ± 0.95

is a more influential surface characteristic on cellular adhesion and proliferation [38, 40] for high surface energy materials such as metal and ceramics. In addition, enhancing the polar component of the surface energy via compositional or surface modifications is also shown to enhance the cellular adhesion and proliferation [41, 42]. Therefore, transparent ceramics and CP-Ti samples have been characterized in terms of polar and dispersive components and total surface energy.

The experimental results shown in Table 2 indicate relatively lower contact angles for transparent ceramics than for CP-Ti, thus improving the wettability of Spinel and ALON®. Since the cell media are water based, the cellular attachment will be relatively poor on any hydrophobic surface with high contact angles. Moreover, a low contact angle of ceramic surfaces suggests their high surface energy, which is another factor that can contribute to better cell attachment [38]. Table 2 also shows different components of surface energy of CP-Ti and transparent ceramics studied in this work. Both the ceramic samples showed significantly higher surface energy than the surface energy of CP-Ti, which is consistent with the observed cell-materials interactions on these samples. However, Spinel with little lower surface energy of 53.64 ± 1.15 mN m^{-1} found to exhibit better living cell density (Fig. 7) than observed on ALON® with a total surface of 55.81 ± 0.65 mN m^{-1}. The enhanced cellular adhesion and proliferation on Spinel is hypothesized due to the positive influence of polar component of the surface energy [41, 42], which is comparable to that of ALON®. Present results show that both Spinel and ALON® transparent ceramics are non-toxic with better cell-materials interactions than CP-Ti. Excellent in vitro wear resistance of these ceramics shows their potential as wear resistant contact surfaces for load bearing implant applications such as in ceramic ball or acetabular cup for hip prosthesis. However, further in vivo studies are needed with these materials to fully understand the tissue-materials interactions.

4 Conclusions

For the first time, commercially available Spinel and ALON® transparent ceramics have been evaluated for their in vitro biocompatibility and wear resistance to explore their potential to be used in contact surfaces for load bearing implant applications. The in vitro biocompatibility study using hFOB cells showed non-toxicity and superior cell-materials interactions of Spinel and ALON® transparent ceramics than CP-Ti. The in vitro wear rate of these ceramics was found to be in the range of 5.3 to 10×10^{-6} mm^3 Nm^{-1}. Among these two ceramics, Spinel exhibited relatively high wear resistance and superior cell-materials interactions than ALON®. The enhanced cellular adhesion and proliferation on Spinel is hypothesized due to the positive influence of polar component of the surface energy.

Acknowledgments Authors would like to acknowledge the financial support from the W. M. Keck Foundation to establish a Biomedical Materials Research Lab at WSU. Authors also acknowledge the financial support from the M. J. Murdock Charitable Trust, National Science Foundation NSF (Grant No. CMMI 0728348) and National Institutes of Health (Grant No. NIH-R01-EB-007351).

References

1. Berry DJ, Harmsen WS, Cabanela ME, Morrey BF. Twenty-five-year survivorship of two thousand consecutive primary Charnley total hip replacements: factors affecting survivorship of acetabular and femoral components. J Bone Joint Surg Am. 2002;84:171–7.
2. Soderman P, Malchau H, Herberts P. Outcome after total hip arthroplasty: part I. General health evaluation in relation to definition of failure in the Swedish National Total Hip Arthoplasty Register. Acta Orthop Scand. 2000;71:354–9.
3. Soderman P, Malchau H, Herberts P, Zugner R, Regner H, Garellick G. Outcome after total hip arthroplasty: part II. Disease-specific follow-up and the Swedish National Total Hip Arthroplasty Register. Acta Orthop Scand. 2001;72:113–9.
4. Bourne RB, Maloney WJ, Wright JG. An AOA critical issue. The outcome of the outcomes movement. J Bone Joint Surg Am. 2004;86:633–40.
5. Ong KL, Mowat FS, Chan N, Lau E, Halpern MT, Kurtz SM. Economic burden of revision hip and knee arthroplasty in Medicare enrollees. Clin Orthop Relat Res. 2006;446:22–8.
6. Kurtz S, Ong K, Lau E, Mowat F, Halpern M. Projections of primary and revision hip and knee arthroplasty in the United States from 2005 to 2030. J Bone Joint Surg Am. 2007;89:780–5.
7. Medley JB, Chan FW, Krygier JJ, Bobyn JD. Comparison of alloys and design in a hip simulator study of metal on metal implants. Clin Orthop. 1996;329(Suppl):S148–59.
8. Klapperich C, Graham J, Pruitt L, Ries MD. Failure of a metal-on-metal total hip arthroplasty from progressive osteolysis. J Arthroplasty. 1999;14:877–81.
9. Cuckler JM, Moore KD, Lombardi AV Jr, McPherson E, Emerson R. Large versus small femoral heads in metal-on-metal total hip arthroplasty. J Arthroplasty. 2004;19(8 Suppl 3):41–4.

10. Vassiliou K, Scholes SC, Unsworth A. Laboratory studies on the tribology of hard bearing hip prostheses: ceramic on ceramic and metal on metal. Proc Inst Mech Eng H. 2007;221:11–20.
11. Lusty PJ, Watson A, Tuke MA, Walter WL, Walter WK, Zicat B. Orientation and wear of the acetabular component in third generation alumina-on-alumina ceramic bearings: an analysis of 33 retrievals. J Bone Joint Surg Br. 2007;89:1158–64.
12. Gates RS, Hsu M, Klaus EE. Tribochemical mechanism of alumina with water. STLE Trib Trans. 1989;32:357–63.
13. Mori S. Adsorption and lubrication. Jpn J Tribol. 1991;36:161–8.
14. Hay JC, White KW. Grain-bridging mechanisms in monolithic alumina and spinel. J Am Ceram Soc. 1993;76(7):1849–54.
15. White KW, Kelkar GP. Evaluation of the crack face bridging mechanism in a $MgAl_2O_4$ spinel. J Am Ceram Soc. 1991;74(7):1732–4.
16. Rhodes WH, Cannon RM, Vasilos T. Stress-corrosion cracking in polycrystalline MgO. In: Bradt RC, Hasselman DPH, Lange FF, editors. Fracture mechanics of ceramics, Vol II. New York: Plenum; 1974. p. 709–33.
17. Berriche Y, Vallayer J, Trabelsi R, Treheux D. Severe wear mechanisms in Al_2O_3-AlON ceramic composites. J Eur Ceram Soc. 2000;20:1311–8.
18. Chevalier J. What future for zirconia as a biomaterial? Biomaterials. 2006;27:535–43.
19. Liang B, Kawanabe K, Ise K, Iida H, Nakamura T. Polyethylene wear against alumina and zirconia heads in cemented total hip arthroplasty. J Arthroplasty. 2007;22:251–7.
20. Brown SS, Green DD, Pezzotti G, Donaldson TK, Clarke IC. Possible triggers for phase transformation in zirconia hip balls. J Biomed Mater Res B. 2008;85:444–52.
21. Tuke M, Taylor A, Roques A, Maul C. 3D linear and volumetric wear measurement on artificial hip joints—validation of a new methodology. Precision Eng. 2010;34:777–83.
22. Calonius O, Saikko V. Force track analysis of contemporary hip simulators. J Biomech. 2002;36:1131–7.
23. Crowninshield RD, Johnston RC, Andrews JG, Brand RA. A biomechanical investigation of the human hip. J Biomech. 1978;11(2):75–85.
24. Bodhak S, Nath S, Basu B. Friction and wear properties of novel HDPE-HAp-Al_2O_3 composites against alumina counterface. J Biomater App. 2009;23:407–33.
25. Sheejaa D, Taya BK, Laua SP, Nung LN. Tribological characterisation of diamond-like carbon coatings on Co–Cr–Mo alloy for orthopaedic applications. Surf Coat Technol. 2001;146–147:410–6.
26. Ribeiro R, Ingole S, Usta M, Bindal C, Ucisik AH, Liang H. Tribological characteristics of boronized niobium for biojoint applications. Vacuum. 2006;80:1341–5.
27. Wheeler KR, James LA. Fatigue behavior of type 316 stainless steel under simulated body conditions. J Biomed Mater Res. 1971;5:267–81.
28. Owens DK, Wendt RC. Estimation of the surface free energy of polymers. J Appl Polym Sci. 1969;13(8):1741–7.
29. Ramesh CS, Khan ARK, Ravikumar N, Savanprabhu P. Prediction of wear coefficient of Al6061–TiO_2 composites. Wear. 2005;259(1–6):602–8.
30. Suh MS, Chae YH, Kim SS. Friction and wear behavior of structural ceramics sliding against zirconia. Wear. 2008;264:800–6.
31. Bull SJ, Kingswell R, Scott KT. The sliding wear of plasma sprayed alumina. Surf Coat Technol. 1996;82:218–25.
32. Saikko V, Keranen J. Wear simulation of alumina-on-alumina prosthetic hip joints using a multidirectional motion pin-on-disk device. J Am Ceram Soc. 2002;85:2785–91.
33. Hsu SM, Shen MC. Ceramic wear maps. Wear. 1996;200:154–75.
34. Kim SS, Kato K, Hokkirigawa K, Abe H. Wear mechanism of ceramic materials in dry rolling friction. J Tribol. 1986;108:522–6.
35. Wang YS, Hsu SM, Munro RG. Ceramics wear maps: alumina. J Soc Trib Lub Eng. 1991;47(1):63–9.
36. Trabelsi R, Orange G, Fantozzi G, Homerin P, Thevenot F. Relationship between mechanical properties and wear resistance of alumina zirconia ceramic composites. J Lub Eng Trib Trans. 1989;32–1:77–84.
37. Medevielle A, Thevenot F, Treheux D. Wear resistance of zirconias: dielectrical approach. Wear. 1997;213:13–20.
38. Bodhak S, Bose S, Bandyopadhyay A. Role of surface charge and wettability on early stage mineralization and bone cell-materials interactions of polarized hydroxyapatite. Acta Biomater. 2009;5:2178–88.
39. Bodhak S, Bose S, Bandyopadhyay A. Electrically polarized HAp coated Ti: in vitro bone cell-material interactions. Acta Biomater. 2010;6:641–65.
40. Hallab NJ, Bundy KJ, O'Connor K, Moses RL, Jacobs JJ. Evaluation of metallic and polymeric biomaterial surface energy and surface roughness characteristics for directed cell adhesion. Tissue Eng. 2001;7:55–72.
41. Redey SA, Razzouk S, Rey C, Bernache-Assollant D, Leroy G, Nardin M, Cournot G. Osteoclast adhesion and activity on synthetic hydroxyapatite, carbonated hydroxyapatite, and natural calcium carbonate: relationship to surface energies. J Biomed Mater Res. 1999;45:140–7.
42. Feng B, Weng J, Yang BC, Qu SX, Zhang XD. Characterization of surface oxide films on titanium and adhesion of osteoblast. Biomater. 2003;24:4663–70.